Anatomical Shape-Based Averaging for Computer Atlas Construction and Craniofacial Anthropometry

J. Márquez Flores[1], I. Bloch[2], T. Bousquet[3], F. Schmitt[2] and C. Grangeat[3],
[1]Image and Vision Lab, CCADET, UNAM, P.O. Box 70-186, México, D.F., 04510
[2]TSI Dept., Ecole Nationale Supérieure des Télécommunications, 46 rue Barrault, 75634 Paris.
[3]Alcatel Alsthom Research, Marcoussis, France

Abstract. We describe original methods for defining and obtaining robust, anatomical shape-based averages of features of the human head anatomy from a normal population. Our goals are computerized atlas construction with representative facial features and craniofacial anthropometry for specific populations. A new method for true-morphological averaging is presented, consisting of a suitable blend of shape-related information for N objects to obtain a progressive average. It is made robust by penalizing, in a morphological sense, the contributions of features less similar to the current average. Morphological error and similarity, as well as penalization, are based on the same paradigm as the morphological averaging. As a case of study, we tested the method for a shape-average of the external ear (the pinna) of 40 individuals.

1. Introduction.

Tele-assisted health services, distributed visualization of anatomical information in digital formats, image-guided surgery, and other activities where biomedical engineering, internet, medical imaging and computer sciences interact, rely more and more on reference information and representative items from large databases. These include: average models from a normal or specific population, anatomical and physiological atlases of human organs, baseline frames of reference, anatomical robust features (e.g. crest-lines of facial features), and phantoms or mannequins, either physical or virtual, for anthropomorphical studies, experimental assessment of different interactions between biological tissue and radiation, acoustic or electromagnetic fields, and simulation of endoscopic or surgical procedures, as well as for augmented-reality interventional medicine.

In particular, anatomical atlases and phantoms in digital formats are playing an increasingly important role in health sciences and biomedical research, as illustrated in Fig. 1. Computer models of anatomy and physiology are becoming more representative of a specific population of individuals, from organs to anthropomorphical features, and bear complex information providing references for identification of common features which are mapped to and from the atlas and then geometrically and photometrically registered. This allows inter-comparisons, and identification of abnormal conditions, for example. Model-based morphometry is thus a timely strategy for detection of disease-specific variants [1]. Multi-modality atlases allow also the assessment of pathology and treatment response, when combining several medical imaging techniques [10]. Since data to be analyzed is multidimensional and complex, atlases provide a reference, a "base truth", and a priori information used for anatomically-driven methods of analysis [2]. Models for

the simulation of surgery procedures and augmented reality are also derived from annotated models. Fig.1 summarizes these and other inter-relations.

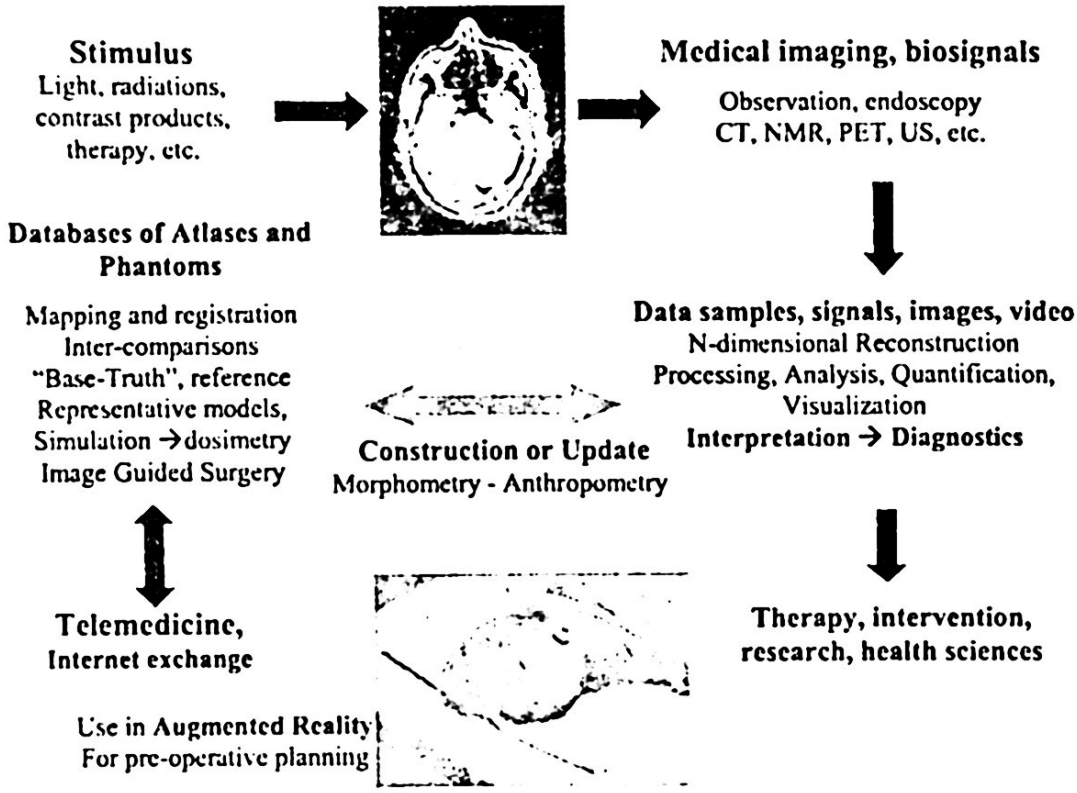

Fig. 1. The roles and context of atlases and phantoms in health sciences. The anatomical slice of the head is from the *Visible Human Project.*

Besides medicine, anatomical models are frequently used in industry, ergonomics and environmental studies. For instance, the shape alone of the head is considered in the study of power absorption and to design safe communication devices [1]. Concerning dosimetry of hand-held phones, the former motivation of the present study, the radio-frequency wave absorption by the human body not only depends on phone terminal positioning, but also depends on anatomical complex features, in particular at the ear and mouth regions. Homogeneous phantoms have been previously used [3], and accuracy improvements up to 2 mm precision resolution from MRI (*Magnetic Resonance Imaging*) scans have been made [4]. However, these studies use a single landmark-based average from army anthropometrical data of male subjects, not representative of the population of mobile phone users. Representative anthropomorphic phantoms from 3D laser-scan acquisitions allow both, simulation and experimental analysis of power absorption in a specific population.

Atlas construction must represent a set of individuals and its variability, by considering contributions from each individual according to some similarity with the true mean. Shape averages of organs and features have been built traditionally by standard arithmetic averaging of the coordinates of specific features, such as sets of landmarks and crest-lines [5]. These constitute averages in the *object domain.* A related approach to atlas construction is that of *statistical shape models* or *active shape models* (or ASM, see [20] and [21]), where statistical properties of several

objects are extracted from landmark information. The statistical or probabilistic and the fuzzy approaches give rise to "soft" models and atlases.

Our goal is to extract a representative instance of a specific (facial) feature from a large population, or from selected subsets. In this paper we describe a morphological, or *shape-based* averaging, generalizing the shape-based interpolation methods from two to N objects. It is an average in the *distance transform domain*, giving rise to "hard" models, where the average itself is an instance of the represented class of features. We also propose a robust rejection or penalization of outliers (rare variations), and test a simple framework for local penalization (local rare variations), in order to take into account only the most common sub-features. As a case of study, we present results for a shape average of the external ear, from a set of 40-individuals of the normal population.

The present work was originated by collaborations between the Image Dept. of the *Ecole Nationale Supérieure des Télécommunications* in Paris and the *Alcatel Corporate Research Center*, (Marcoussis laboratories, France). Details of the former project on automatic construction of head models are found in [3], [6] and [19].

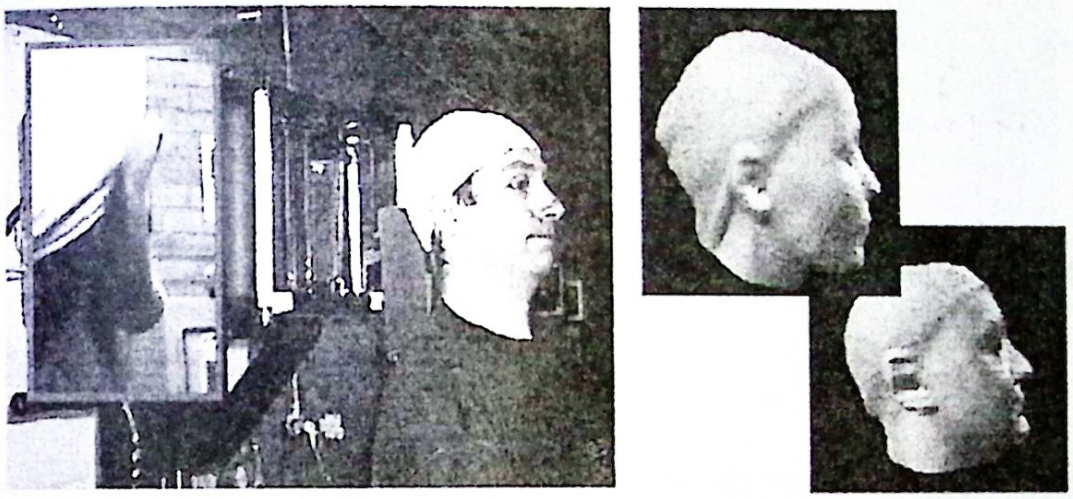

Fig. 2. Laser scan acquisitions of 40 people, with ear collapsed and free (inset). At *right*, renderings of the mesh models at 8mm resolution from cylindrical depth-range images.

2. Methods

2.1. Laser-scan acquisition protocol.

Laser-scan acquisitions were obtained from human heads and processed for the construction of anthropomorphical phantoms, required formerly for dosimetry studies of hand-held mobile phones. Fig. 2 shows the acquisition setup, with a 3D laser scanner from *Cyberware* [7], which rotates around the head, producing distance information of the 3D relief. In total, 40 subjects were scanned, with 12 women in the final sample. Raw data was converted to cylindrical range images at 480×580×5-byte (floating point) resolution, and several image processing techniques were applied for 3D-model construction [19], in order to filter out artifacts and noise, preserving accuracy, and to locate morphological features in *image space* and then in *object*

space [8]. A triangulated surface was obtained for rendering, and for CAD, in order to build physical phantoms. Interactive 3D visualization of mesh models is based on the VRML (*Virtual Reality Modeling Language*) format, and was used for browsing the models in a tele-collaboration framework across Internet. A voxelized version was also produced (Fig. 3-a, b) for processing and for finite-element simulations.

In Fig. 3 a-b, two voxel-volume heads are visualized, with discrete labels in color locating ear, no-ear, and interpolated intruding and extruding tissue. Such volumes were prepared for simulation of radiofrequency-field interactions with the head tissue. Small colored isolated voxels arise from the randomized diagonal swapping of the Eulerian triangulation before voxelization, and they are of no importance.

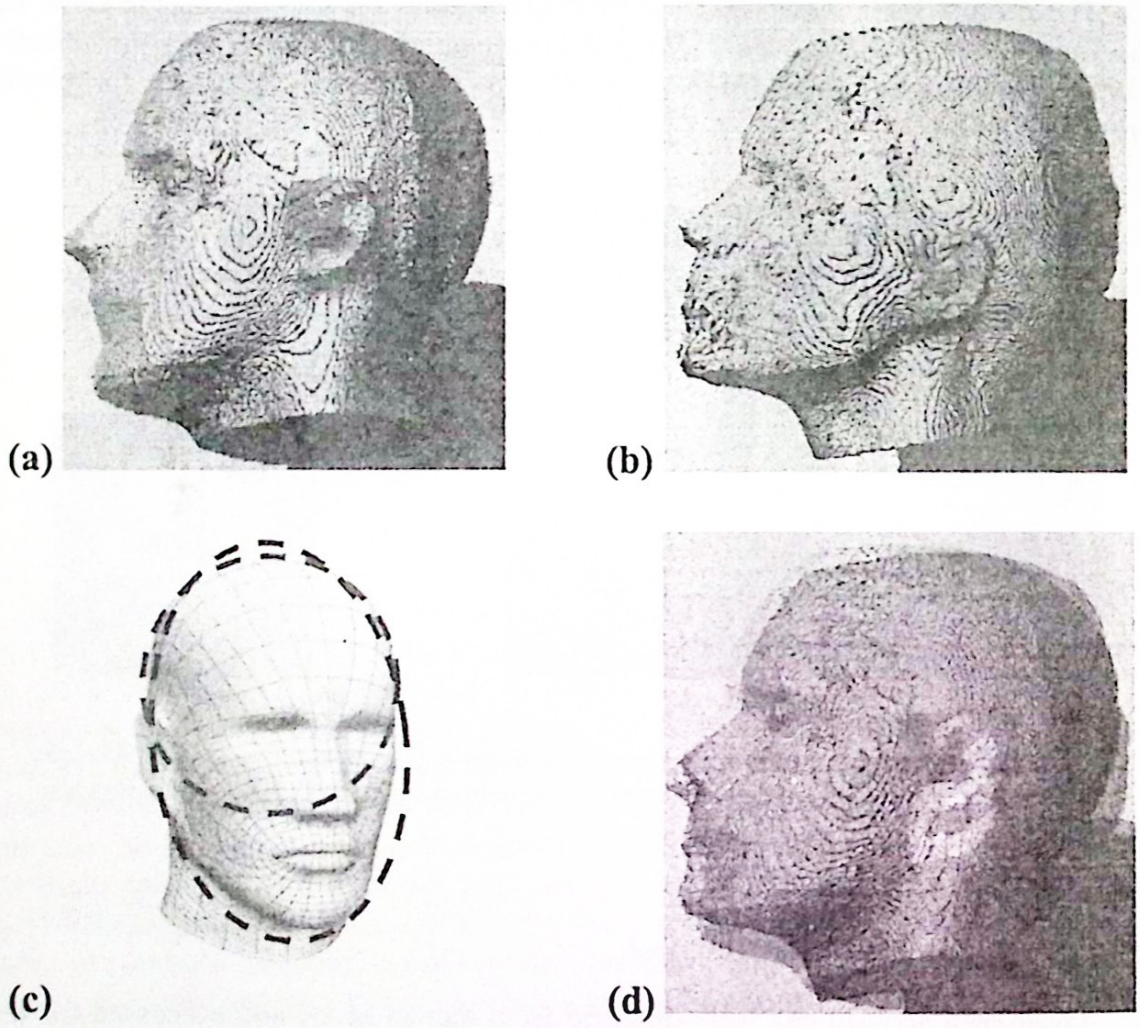

Fig. 3. Even if two heads (a) and (b) from the database are geometrically registered and scaled by (c) robust principal-axis alignment (ellipsoidal, first-order model, in red; zero-order in blue), a 3D superposition of two "aligned" heads (d) shows features at very different positions (order zero provides the best alignement of the auricular-temporal region).

The ear region was then isolated and replaced by a *bilinearly-blended Coons patch surface* that interpolates the skull, using the range-image information around the ear, synthesizing the Coons spline by the tensor product of orthogonal profiles. A baseline implicit surface was thus defined (see also Fig. 3-a,b), useful for measuring

features of human heads; in particular, an average thickness of the ear was estimated on 40 individuals; further details are found in [9]. Head models "with" or "without" ears were built for assessing dosimetry and anthropometry problems. The range-image representation was also convenient for other manipulations and measurements, since 3D information is displayed in the *Mercator cylindrical projection* as a gray-level image. This projection also simplified the interpolation of the auricular-temporal region, and the 3D geometric registration, as explained next.

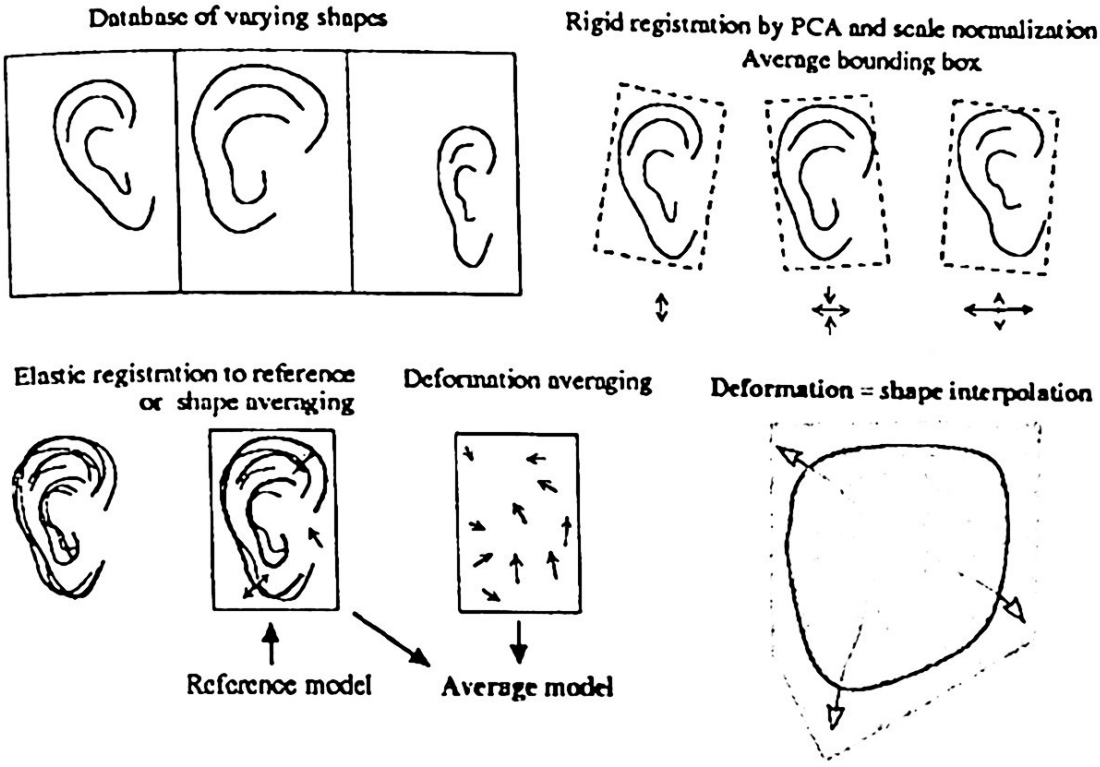

Fig. 4. Simplified process for the construction of average models. The concept of morphological average comes from that of morphological interpolation between two similar shapes (*bottom right*), where the transformation has to deal with the correspondence problem.

2.2. Feature-Based Registration.

Morphological tasks such as comparisons and averaging require first a geometrical correspondence of datasets in a common frame of reference. Non-linear registration of matching features is a challenge for atlas construction, in particular for the highly varying shape of human anatomy [10], and the external ears are a typical example. In a first approach we used a global alignment of principal axes for the bounding box of the auricular-temporal region. Note that a global alignment of the full heads is not useful, as illustrated in Fig. 3, where the ears are far from superposing. A similar problem arises when global alignment is confined to the bounding box of the ears. A better approach was to extract robust features of the ears, such as the external crest-lines, available from the depth-range images. In the case of brain structures, the atlas construction process has been adapted to multi-modal imaging [5], and a similar framework is illustrated in Fig. 4, where we have integrated

our approach considering shape-based interpolation (bottom right) as a deformation. Note that an affine registration is required, since ears vary in size and shape.

We used the *Iterated Closest Point* (ICP) algorithm [11], which is a general purpose, shape-based registration. The steps for geometrical registration comprise:

- External ear (pinna) contour (crest lines) extraction, from the depth-range images of each head before mesh construction.
- Bounding-box extraction in 3D for each contour.
- Principal Component Analysis to obtain the 3D-inertia axes.
- Principal axes alignment (preliminary step for ICP alignment).
- Affine registration transform of contours by the ICP algorithm.
- Average transformation.
- Average ROI (bounding-box); average scale calculation.
- Scale normalization of all heads.
- Hi-resolution mesh (~2mm) and mesh transformation.
- Voxelization of ROIs. The registered set is ready for averaging.

The same procedure was applied to the implicit surfaces underlying the pinna. Fig. 5 shows the feature-based registration, using the crest-lines of the ear borders, and their bounding boxes. Cylindrical coordinates of data from the laser-scanner acquisitions allow to work with 3D surfaces data as 2D depth-range images, thus a "2D" bounding box is shown, but the process was done in 3D, before mesh bulding and voxelization. Matching of local features is only approximate, and there may be several deformation paths, or, equivalently, several interpolation paths, as illustrated by the slightly curved arrows of the morphing process of Fig. 4, bottom right. Energy-minimization criteria have been proposed to obtain an optimal interpolation [12], but its computer complexity is too high even for low resolution data, and there is no evidence for deformation-energy processes to explain inter-individual variations.

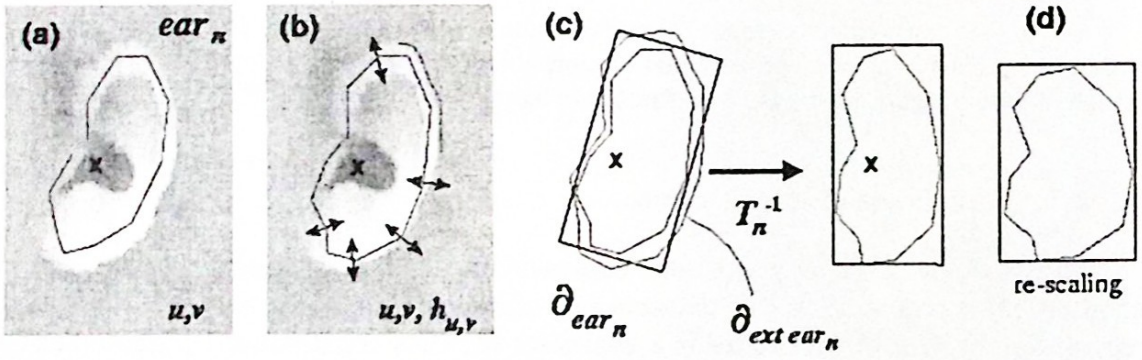

Fig. 5. Local, inter-individual registration of the external ear region was based on affine registration of robust features: the crest-lines of the ear borders from the range-images (a,b). Rotation (c) and homogeneous scaling on the 3D bounding box (the figure shows a 2D projection) was done using the average bounding box as reference (d).

The resulting alignment, for a sample of 5 ear borders, is illustrated in Fig. 6. In spite of original registration of the heads during acquisitions, the ear shapes have quite different positions and orientations, besides shape and size variation. An average bounding box provided a frame of reference and a common scale for all ears.

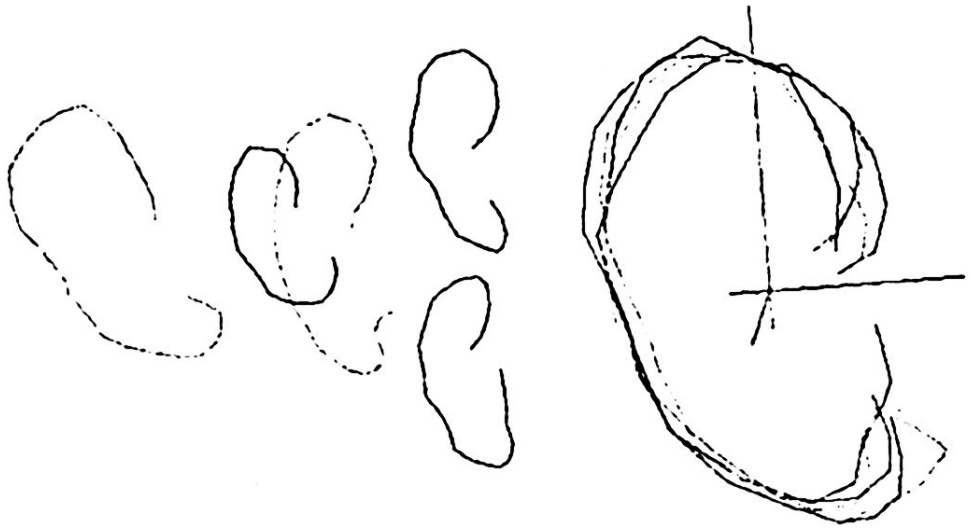

Fig. 6. Feature-based registration. (*Left*) 3D-reference contours (border of the ear) before affine registration. (*Right*) Superposed contours after homogeneous scaling and registration by *Principal Component Analysis*, i.e. alignment of each set of 3D axes of inertia.

2.3. From morphological interpolation to shape-averaging.

Morphological interpolation techniques have been introduced in several fields, from industrial design, to medical imaging, with the common goal of effectively interpolating shape profiles, and binary shapes between consecutive image slices, as opposing to signal interpolation in a point-to-point basis on gray-level images. Specific techniques are described in [13], [14], [15]. The concepts of metamorphosis and morphing, are special cases, when interpolating very different, unrelated shapes, with arbitrary correspondence criteria [16], [23]. Slice-image, linear interpolation between two similar shapes is usually done as follows.

Let A, B be two discrete objects and let $\mathbf{D}_A$ y $\mathbf{D}_B$ their discrete, signed distance fields (also known as distance transforms), then the linear *blending* $\mathbf{D}_\alpha = (1-\alpha)\,\mathbf{D}_A + \alpha\,\mathbf{D}_B$ provides a simple way to interpolate an "intermediary" object $\mathbf{D}_\alpha$ between both A, B (these interpolation process is popularly known as "morphing"). The corresponding shape is extracted from iso-surface at a threshold distance zero. The last is also known as a zero-level set. The exact average shape corresponds to $\alpha=1/2$. Since it is a linear operation, a third shape C allows conceptualizing a triangle in "shape space" (or more properly, the distance-transform domain) whose vertices are A, B and C, and the central interpolated shape is a shape-based average. Thus, we introduce a N-object average, first listing the following:

Definitions

$\mathcal{V}$ Digital scene, usually a N×M×L volume. The volume $\mathcal{V}$ may be also a *scalar field*, it is, at point (x,y,z), the quantity $d = \mathcal{V}(x,y,z)$ is a scalar.

V Discrete object in $\mathcal{V}$ (e.g., digital information of an anatomical structure, represented by an array of scalar or vector values, or a mesh structure).

∂V Boundary of the object V (its discrete surface). It depends on segmentation or selection criterion (e.g. external surface of an organ, bone, arteries, etc.).

$\mathbf{D}(\partial V)$ Signed distance field (a discrete volume with scalar values) associated to boundary ∂V. Note that $\mathbf{D}(\partial V)$ is a scalar field. It is also called the (Euclidean) *Distance Transform*. For simplicity we use the notation $\mathbf{D}_V$.

$L_{d=d0}(\mathcal{V})$ Level-set (iso-surface at $d=d_0$) of a scalar field. Note that under certain conditions, at distance $d=0$ it is possible to define $L_{d=0}$ as an inverse transform: $\partial V = L_{d=0}(\mathbf{D}(\partial V))$.

$< x_i >$ Conventional average (expected value) of N simple data x_i.

$\overline{\partial V}$ or $\ll V_i \gg$ (Any) morphological average of N objects V_i, to be defined later.

$\ll V_i \gg_R$ Robust morphological average. This shape is the basis for a representative model or *atlas*, when labels and attribute information are incorporated.

With the latter notation, we introduce the Euclidean (in the case of Euclidean metric), and the Chamfer (in the case of discrete metric for chamfer-distance transforms) *morphological average* based on the signed distance field associated to the boundaries ∂V_i of each object V_i:

$$\overline{\partial V} = \ll V_i \gg = L_{d=0} \left\{ \sum_{i=1}^{N} \mathbf{D}(\partial V_i) \right\} \qquad \text{eq. (1)}$$

The zero-level set is the external iso-surface (or boundary) of the average object. Both notations correspond to two interpretations of the result, as a boundary $\overline{\partial V}$ of an object V and as a morphological average among several instances V_i.

The averaging can be made "robust" in a statistical sense, when each shape-term of the sum is penalized according to its similarity to the current average, and then recalculating the latter (see Fig. 7). Let $\{ w_i \}$ the normalized set of weights; the starting condition is an homogeneous contribution such that $\Sigma_N w_i = 1$, and we define a *robust (Euclidean or Chamfer) morphological average*:

$$\ll V_i \gg_R = L_{d=0} \left\{ \sum_{i=1}^{N} w_i \mathbf{D}(\partial V_i) \right\} \qquad \text{eq. (2)}$$

An iterative method allows to find an optimal set $\{ w_i \}$ from an error measure to be minimized when comparing ∂V_i with $\ll V_i \gg_R$. The error space is for the moment assumed to be convex (no local minima), but a better analysis needs to be done.

A mechanism to compare 3D objects is to use the distance fields of each shape, in order to define a "morphological error", which can be based on a squared difference, voxel-to-voxel and for each scalar field. For all voxel values

$u(x,y,z) \in \mathbf{D}(\partial V_i)$ and its corresponding value $v(x,y,z) \in \left\{ \sum_{i=1}^{N} w_i \mathbf{D}(\partial V_i) \right\}$,

the volume set $Err^2(V_i)$ is formed with the voxel values:

$$err^2(x,y,z) = \left[v(x,y,z) - u(x,y,z)\right]^2 \qquad \text{eq. (3)}$$

Note that Err^2 (V_i) is a scalar scene. Integrating in all (x,y,z) we obtain a global measure of error, permitting evaluation of a weight for ∂V_i when averaging at iteration n+1. Note that local integration on any specific region, allows evaluating the contribution to global error for that region. Thus, weights w_i may be variable, either point to point, locally, or even by very specific ROI's (a facial feature, for example).

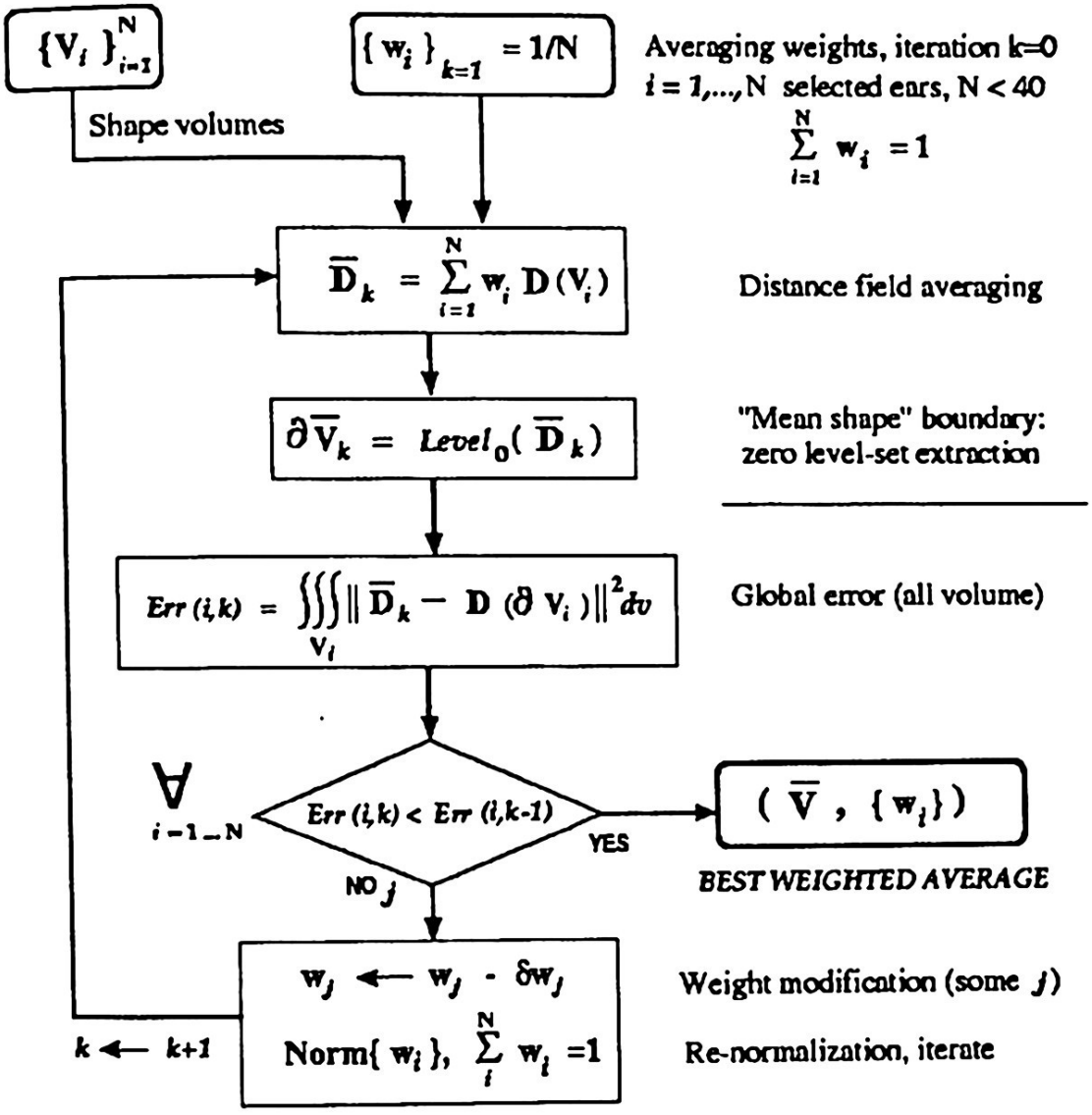

Fig. 7. The robust shape-based averaging algorithm for a set of N shapes $\{V_i\}$. The set of weights $\{w_i\}$ is shift-invariant, but may also be a function of position (x,y,z), or assigned locally to each sub-feature of V_i.

An incrementing algorithm, modifying one w_i at a time, was devised to avoid re-calculating the distance-field average again, by subtracting the contribution of ∂V_i at iteration k-1 and updating it with the new value for w_i. A similar approach works for new shapes to be included in the average, which is the essence of a population atlas which is more representative at each contribution.

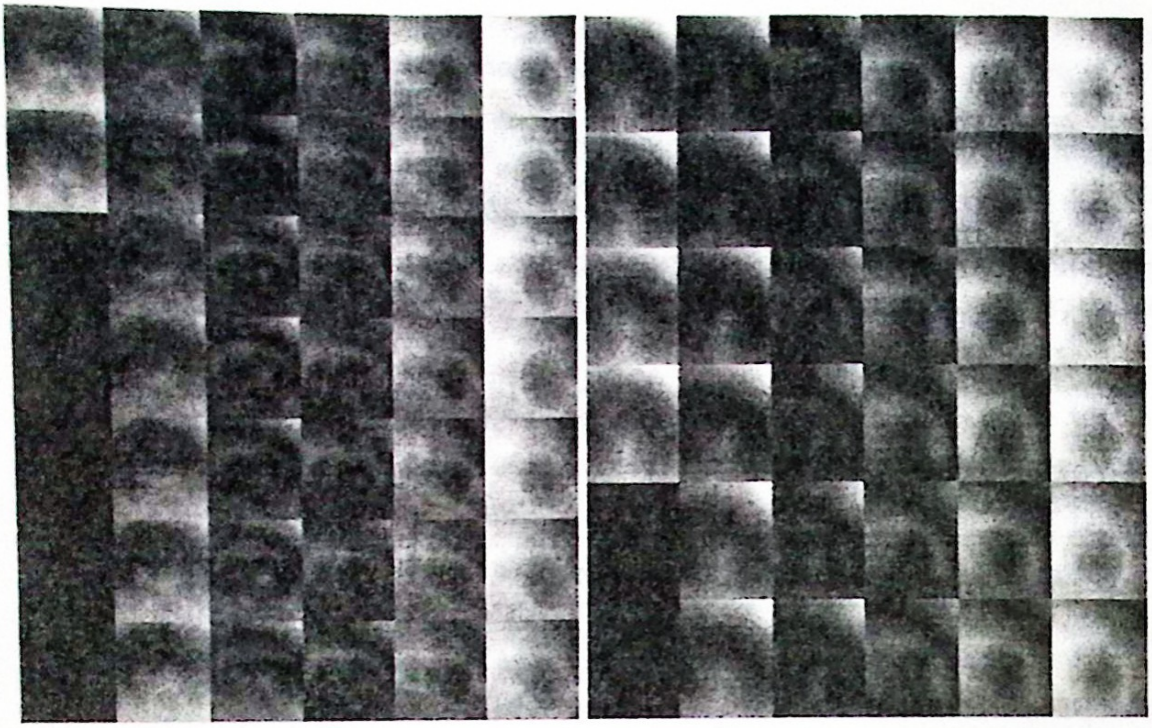

Fig. 8. (*Left*) Unsigned 3D distance field of the boundary of one human ear. (*Right*) Idem, distance field averaged over 40 individuals.

Figure 9 (right), shows a 3D rendering of the resulting average shape, extracting a triangular mesh from the voxel-representation results, and its interpolated, implicit, base surface (middle surface, in sky blue), once integrated to a generic phantom.

3. Results and Discussion

Figure 8-a shows a few Z-slices of the unsigned 3D-distance field of the surface boundary of one human ear (binary information). The "unsigned" version shown, i.e. |d|, is a display enhancement by look-up tables, to make visible the cross sections of the 3D boundary of the ear and to better display the field gradient. Fig. 8-b shows also slices (not the same Z-levels that Fig, 6-a) of the average distance field within 2 mm of global error over 40 individuals. The level set at Z=0 (gray level black in the figures) corresponds to the boundary of the original shape *i* and the averaged shape. Note that averaging on 40 shapes produces a smoothed shape. There remains the question of validating the average as a feasible human ear, and the method could be refined by constraining the error minimization while respecting some ear-ness criterion. An answer to the question "to what extend the shape-based average is a valid human ear" lies on the size of local mismatches: the average is an interpolation among real ear features, provided that their extrema correspond one-to-one. A correspondence mismatch implies an invalid local interpolation of at most the size of that mismatch. Non-rigid registration may help to improve correspondence matching.

To reproduce the situation of users of mobile-phones, the acquisitions comprised a version with the ear collapsed against the skull. The thickness of the corresponding averaged ear, measured by methods reported in [9] was about 6.2 ± 2.5 mm, and

agrees well with the measure of this thickness in the *Standard Anthropomorphic Model* [17], obtained by different methods.

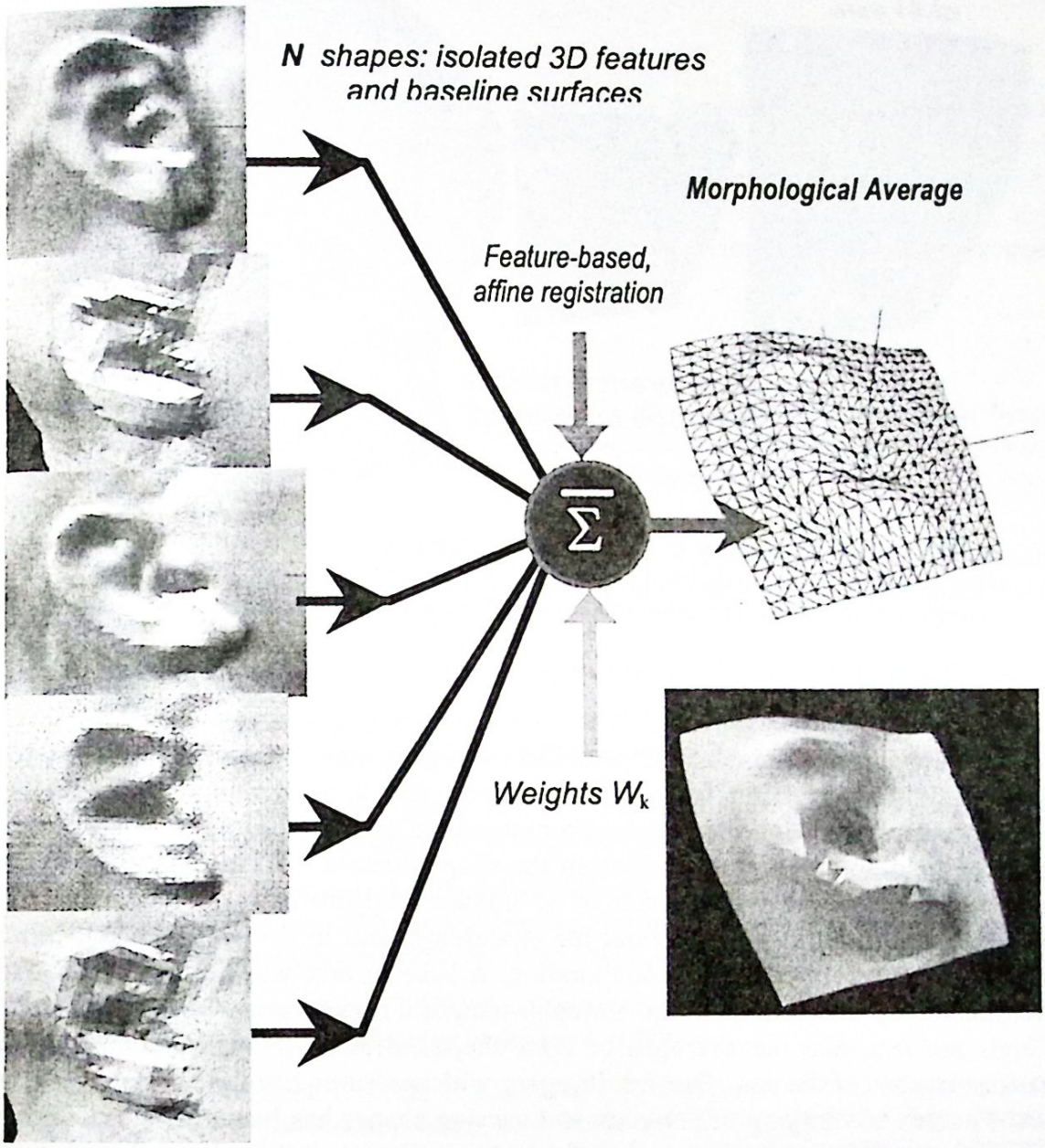

Fig. 9. (*Right*) Elements for the construction of an anatomical, robust, morphological-average of the ear from 40 individuals. Features are the border lines of Fig. 6. (*Left*) A 3D rendering of the resulting average shape (triangular-mesh representation).

The present approach also permitted averaging the implicit surface that interpolates the skull, described in [9]. Thus, a morphological-average of the head "without ears" can be obtained, too, and Fig. 10 illustrates the construction of morphological averages of the ear and its corresponding average implicit-base surface, integrated to a generic head phantom (virtual as well as physical) for dosimetry studies.

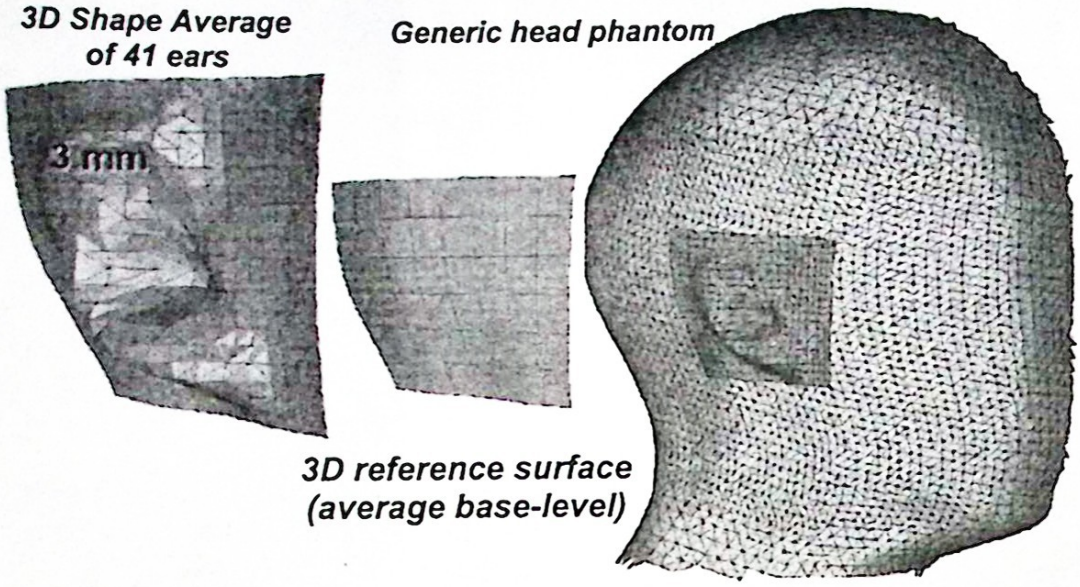

Fig. 10. Morphological averages of the ear and its corresponding average implicit-base surface, integrated both to a generic head phantom. The measure "*3mm*" corresponds only to a subregion of the pinna, and other thickness values, at different regions, were obtained.

4. Conclusions.

An innovative method of shape-based averaging was presented. It blends the distance-field information from several shapes, and a robust implementation was obtained, applying similar ideas to error measures and similarity, calculated in the distance-field domain, rather than from the shape domain. To test our methods, an average of the ear from a database of 40 human head profiles was obtained. The database was build in voxel format for processing, and in the web-oriented format VRML, for browsing and tele-collaboration. A base surface was defined an obtained from boundary information at the auricular-temporal region, using *bilinearly-blended Coons patches*, and the averages of both shapes allowed to measure thickness at various regions of the ear. Our results agree with measures from the widely accepted SAM model. Averaging of complex and varying shapes has been difficult without a reliable geometric registration, and the implicit Coons surface has alleviated this problem, providing also a baseline for error quantification during registration. A feature-based approach, using the crest-lines of the external ear, was also used for a more robust registration, before averaging in the distance field domain. Registration may be based also on distance fields, a procedure known as "chamfer matching", and a combination with line feature-based registration is possible by modulating distance fields. Future work comprises these enhancements, as well as averaging methods including not only weighted distance fields, but also the fields of non-rigid deformations.

The construction of models of anatomical features from a specific population is becoming a key-step towards digital atlases which integrate annotated information, morphometry and even physiology (e.g. functional imaging). Computer phantoms of facial features from these models will be useful in simulation of craniofacial

reconstruction, anthropometry and to build virtual and physical prostheses, which can be made highly customized, at least to a local population.

Acknowledgments

The present work resulted from collaborations between the *Ecole Nationale Supérieure des Télécommunications*, Paris, and *the Alcatel Corporate Research Center, (Marcoussis laboratories).* We gratefully acknowledge the assistance of Dr. M. Nahas, from the Paris VII University for laser scanning assistance. We also acknowledge M. Ackerman of the National Institutes of Health for providing access to the *Visible Human Project* dataset.

References

[1] P. Thompson, M. Mega, K. Narr, E. Sowell, R. Blanton and A. Toga. Brain Image Analysis and Atlas Construction. In: Milan Sonka and J. Michael Fitzpatrick (editors) Handbook of Medical Imaging, Vol. 2, Medical Image Processing and Analysis. SPIE Press 2000, pp. 1061-1129.

[2] P. Thompson, and A. Toga. *Brain Warping* (edited by A. Toga), ch. Anatomically-Driven Startegies for High-Dimensional Brain Image Warping and Pathology Detection, pp. 311-336. Acad. Press, 1998.

[3] C. Grangeat et al., *Alcatel Telecommunications Review,* 4th Quarter (1998), pp.298-304.

[4] J. Wiart et al., Proceedings of the *Second World Congress for Electricity and Magnetism in Biology and Medicine,* Bologna, June (1997), Plenum Press.

[5] G. Subsol, J.F. Thirion, N. Ayache. (1992),*"First steps towards automatic building of anatomical atlases."* Research Report RR-2216, INRIA Rocquancourt, France, mars 1994.

[6] J. Márquez, T. Bousquet, I. Bloch, F. Schmitt and C. Grangeat. Poster # 25, *BioElectroMagnetics Society, 22th Annual Meeting,* Technical University, Munich, Germany. Abstract Book (Technical University, Munich): June 9-16, (2000). pp. 123.

[7] Inc. Cyberware Laboratory, "4020/rgb 3d scanner with color digitizer", available at: http://www.cyberware.com/pressReleases/index.html, (1990).

[8] J. Márquez, T. Bousquet, I. Bloch, F. Schmitt and C. Grangeat. (2000b), "*Construction of Human Head Models for Anthropometry and Dosimetry Studies of Hand-Held Phones.*" Revista Mexicana de Ingeniería Biomédica. Vol. XXI, No. 4, diciembre de 2000. pp. 120-128.

[9] Jorge Márquez, Isabelle Bloch y Francis Schmitt. (2003), *"Base Surface Definition for the Morphometry of the Ear in Phantoms of Human Heads."* Session 2.2.2, Poster #1113, *2nd IEEE International Symposium on Biomedical Imaging*, Cancún, Mexico, September 15-20 2003.

[10] P. Thompson, R. Woods, M. Mega and A. Toga. Mathematical/Computational Challenges in Creating Population-Based Brain Atlases. Human Brain Mapping, vol. 9, pp. 811-90, February 2000.

[11] Besl Paul J and Neil D. McKay. A Method for Registration of 3-D Shapes. IEEE Transactions on Pattern Analysis and Machine Intelligence, 14 (2), Feb. 1992, pp. 239-256.

[12] E. Bribiesca, Measuring 3-d shape similarity using progressive transformations, Pattern Recognition, 29 (1996).

[13] G. J. Grevera and J.K. Udupa, "Shape-Based Interpolation of Multidimensional Grey-Level Images," IEEE Trans. Med. Imag., Vol. 15, No. 6, pp. 882-892 (1996).

[14] G. T. Herman, J. Zheng and C. A. Bucholtz, "Shape-Based Interpolation," IEEE Comp. Graph. Appl., Vol. 12, No.3, pp. 69-79 (1992).

[15] S. P. Raya and J. K. Udupa. "Shape-Based Interpolation of Multidimensional Objects", IEEE Trans. Med. Imag., Vol. 9, No. 1, pp. 32-42 (1990).

[16] D. Cohen-Or, D. Levin and A. Solomovici. Three-Dimensional Distance Field Metamorphosis. ACM Transactions on Graphics, 17, 1998, pp. 116-141.

[17] - "SAM - the Standard Anthropomorphic Model", Information at: http://www.sam-phantom.com/SAMinfo.htm.

[18] Geisen G.R., Mason C.P., Houston V.L., Whitestone J.J., McQuiston B.K. and A.c Beattie, (1995), "Automatic detection, identification and registration of anatomical landmarks," Proc. Human Factors and Ergonomics Soc. Vol. 2, pp. 750-753, 1995.

[19] J. Márquez, I. Bloch and F. Schmitt. "IPCYL : Logiciels de traitement de données cylindriques et images en profondeur, MakeTri et Voxelize: maillage triangulaire et voxelization pour la création de fantômes antropométriques". (Vers. 1.0). *Dept. IMAGES, ENST*, Paris, october (1999).

[20] T. F. Cootes, C. J. Taylor, D. H. Cooper and J. Graham, "Active Shape Models – Their training and applications", *Comp. Vis. Image Understand.*, vol. 61, no. 1, pp. 38-59, 1995.

[21] A. F. Frangi, D. Rueckert, J. Schnabel and W. Niessen, "Automatic Construction of Multiple-Object Three-Dimensional Statistical Shape Models: Application to Cardiac Modeling", *IEEE Transactions on Medical Imaging*, vol. 21, no. 9, September 2002.

[23] Payne, B.A.; Toga, A.W.; (1992) "*Distance field manipulation of surface models.*" Computer Graphics and Applications, IEEE , Volume: 12 Issue: 1 , Jan. 1992. Page(s): 65 -71.